ACS Photonics

pubs.acs.org/journal/apchd5 Article

Tunable Frequency Filter Based on Twisted Bilayer Photonic Crystal Slabs

Beicheng Lou* and Shanhui Fan*

Cite This: https://doi.org/10.1021/acsphotonics.1c01263 Read Online

ACCESS | Metrics & More | Article Recommendations | Supporting Information

ABSTRACT: We introduce a tunable narrow-band-stop frequency filter based on twisted bilayer photonic crystal slabs. The operation of the filter is based on the guided resonance of the slabs. We choose to operate in a regime where the operating wavelength is significantly larger than the periodicity of the individual photonic crystal slabs, such that all the resonances in the operating frequency range arise from the Moire periodicity, and hence, their resonant frequencies are strongly dependent upon the twist angle. We also show that a desired notch filter line shape can be achieved by introducing additional uniform slabs and that the filter can operate without diffraction loss and is polarization-independent. Such a filter may be potentially important for communication and signal processing applications.

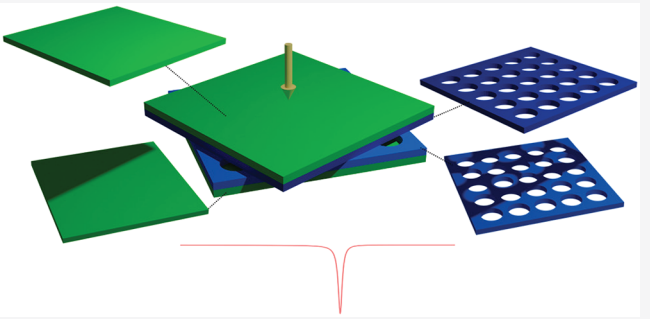

KEYWORDS: *filter, Moire, twisted bilayer photonic crystal*

Inspired by the recent discoveries of novel electronic properties in twisted bilayer graphene,[1,2] there has been a surge of interest in twisted photonic structures consisting of a thin film on top of another.[3−13] One major attraction of these structures is that their optical properties can depend strongly on the in-plane twist angle between the films, which enables applications such as tunable circular dichroism,[10−12] tunable thermal emission,[8] and tunable lens focus.[13]

Our aim here is to create a tunable narrow-band filter based on such twisted photonic structures. A single layer of photonic crystal slab (Figure 1a) can operate as a narrow-band filter for light at normal incidence, based on the guided resonance that the slab supports. In a twisted photonic structure consisting of two such layers (Figure 1c), the periodicity of the Moire pattern becomes strongly dependent on the twist angle. Thus, it has been shown in previous work[5] that some resonant frequencies can be strongly controlled by the twist angle. However, there are several challenges in applying the structure of previous work[5] for creating a tunable narrow-band filter. In the operating frequency range, there are many resonances with frequencies close to each other, among which a significant portion have resonant frequencies independent of the twist angle. Thus, the spectral response of the structure is very complicated. Moreover, the twist can introduce additional diffraction channels, whereas many filter applications need all diffractions to be suppressed.

To overcome the challenges as outlined above, in this paper we re-examine the twisted bilayer photonic crystal slab structure, such as the structure shown in Figure 1c, toward the tunable filter application. Our work here differs from previous work[5] in several important aspects. Foremost, here we consider a small-periodicity regime where the periodicity of each individual layer is significantly smaller than the operating wavelength. Operating in such a small-periodicity regime ensures that the guided resonance cannot be excited through the periodicity of a single layer and, instead, can only be excited through the Moire pattern formed in the twisted structure. Thus, in this regime, the resonance response of the structure becomes far simpler, and moreover, all resonances become tunable by the twist angle. Operating in this regime also helps in suppressing the diffraction. The desired resonant filter lineshapes can be obtained with the use of additional uniform dielectric layers. As a result, we can design narrow-band filters with only a single resonance response in a relatively broad operating frequency range, with the resonant frequency strongly tunable by varying the twist angle. Such a narrow-band filter may be potentially important for communication and signal processing applications.

RESULTS AND DISCUSSION

A photonic crystal slab (Figure 1a) supports guided resonances, which are strongly confined within the structure and can couple to external radiation.[14] The guided resonances typically manifest as narrow spectral features with Fano lineshapes in the

Received: August 19, 2021

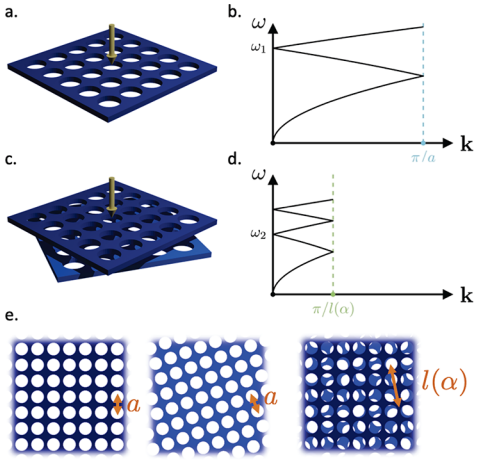

Figure 1. (a) A single-layer photonic crystal slab consisting of a square lattice of air holes in a high-index dielectric slab. (b) Illustration of band folding for the single-layer photonic crystal. The wavevector is along an in-plane direction of the photonic crystal slab. a is the lattice constant of a single layer, as shown in (e). (c) A twisted bilayer photonic crystal slab structure. (d) Illustration of band folding for the twisted bilayer photonic crystal structure. The wavevector is along an in-plane direction of the photonic crystal slabs. $l(\alpha)$ is a Moire periodicity as shown in (e). (e) Illustration of the Moire pattern formed by the two photonic crystal layers, where the Moire period as a function of twist angle α is $l(\alpha) = [2\sin(\alpha/2)]^{-1}a$.

transmission spectrum of the slab. These features have been widely explored for filter applications.[15−26]

The frequencies of guided resonances in a photonic crystal slab can be understood from a band-folding picture. As illustrated in Figure 1b, the band structure for a photonic crystal slab could be viewed as folding the guided mode band of an effective homogeneous slab into the first Brillouin zone of the photonic crystal. Normally the incident plane wave couples to the guided resonance with an in-plane wavevector $k = 0$. For a slab consisting of a square lattice of air holes, the lowest nonzero resonant frequency at $k = 0$ is approximately

$$\omega_1 = \frac{2\pi c}{n_{\text{eff}} a} \tag{1}$$

where c is the speed of light, a is the lattice constant, and n_{eff} is the effective refractive index of the homogeneous slab.[14] One benefit of exploiting this lowest-order guided resonance is that all diffractions are evanescent. The effective refractive index is $n_{\text{eff}} > 1$, while the lowest-order diffraction has a wavevector of $|\mathbf{g}| = \frac{2\pi}{a}$. Therefore, $\omega_1 < 2\pi c/a = c|\mathbf{g}|$, and the slab is nondiffracting for normally incident light at ω_1.

Based on eq 1, two natural ways to tune the resonant frequency are by changing the lattice constant a[19] and by changing the effective refractive index n_{eff}.[18] However, in a single slab, neither the lattice constant nor the effective refractive index can be changed substantially. To achieve more flexible tuning, one could employ two photonic crystal slabs and tune the resonant frequency by adjusting the displacement between the slabs.[27] However, in this approach, the frequency range where the system can operate as a tunable narrow-band filter is restricted to the line width of the guided resonance of a single slab.

In this paper, we consider a tunable narrow-band filter based on twisted bilayer photonic crystal slabs. Analogous to a single photonic crystal slab as discussed above, the frequency of the guided resonance at $k = 0$ of the twisted bilayer structure can also be obtained from a band folding picture, as illustrated in Figure 1c,d. The twisted bilayer photonic crystal slabs is quasi-periodic with Moire pattern (Figure 1e). The Moire periodicity leads to band folding into the corresponding Moire Brillouin zone. At $k = 0$, the lowest nonzero resonant frequency is approximately:

$$\omega_2 = \frac{2\pi c}{n_{\text{eff}} l(\alpha)} \tag{2}$$

Here the Moire period $l(\alpha) = [2\sin(\alpha/2)]^{-1}a$ can be easily tuned by varying the twist angle α between the two layers. Operating at a frequency near this guided resonance at ω_2 also has the benefit that the lowest-order diffractions at wavevector $|\mathbf{g}| = \frac{2\pi}{l(\alpha)}$ are evanescent.

The existence of a tunable guided resonance due to the Moire periodicity has been noted in previous work.[5,8] However, the existing work does not naturally lead to the design of a tunable filter. As an example, we consider a structure, as illustrated in Figure 2. The structure consists of two homogeneous slabs

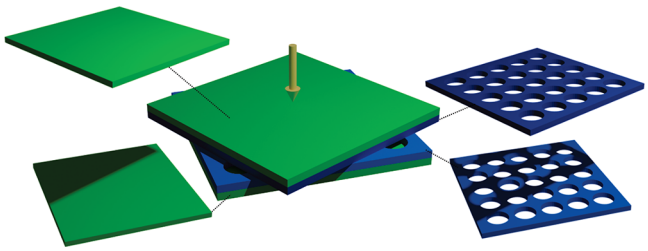

Figure 2. Structure considered in this paper consists of two homogeneous slabs sandwiching two photonic crystal slabs with circular air holes in the square lattice. Each slab is of dielectric constant $\epsilon_r = 12$, with the thickness being $0.2a$, and the hole radius is $0.4a$, where a is the lattice constant. There is no gap between all neighboring layers.

sandwiching two photonic crystal slabs. Each slab is of a dielectric constant of 12, with a thickness of $0.2a$. The photonic crystal slabs consist of circular air holes in a square lattice. The hole radius is $0.4a$, where a is the lattice constant. The lattices of the two photonic crystal slabs are twisted against each other by an angle α. The twist angle can be tuned. We will subsequently use the same structure but at a different frequency range for our design of a tunable filter. Here we consider the frequency range from $0.3c/a$ to $0.5c/a$, which is similar to the frequency range probed in previous work.[5]

Figure 3a shows the transmission coefficients as a function of frequency and twist angle, for such a structure in the frequency range from $0.3c/a$ to $0.5c/a$ for normally incident light. Here, the transmission coefficients are determined by summing the power in all diffraction orders. At each twist angle, the transmission spectrum of the structure exhibits sharp spectral features corresponding to the guided resonances. There are several challenges that make the transmission spectrum shown in Figure 3 undesirable for tunable filter applications. Within the frequency range there are a substantial number of resonances, leading to a complex transmission spectrum, as shown in Figure 4b. Also, while some of these guided resonances display a strong dependence on the twist angle, others are twist-angle-independent. The frequencies of these two classes of resonances are close to each other, which makes it difficult to construct a clean tunable filter response.

https://doi.org/10.1021/acsphotonics.1c01263
ACS Photonics XXXX, XXX, XXX−XXX

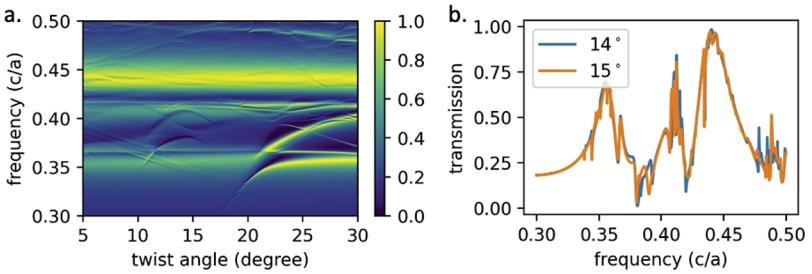

Figure 3. Transmission properties for the structure shown in Figure 2 in the frequency range from $0.3c/a$ to $0.5c/a$ for various twist angles. Here the transmission is obtained by summing the power over all diffraction channels. The incident light is right circularly polarized. (a) Transmission coefficients as a function of frequency and twist angle. (b) Transmission spectra for two twist angles.

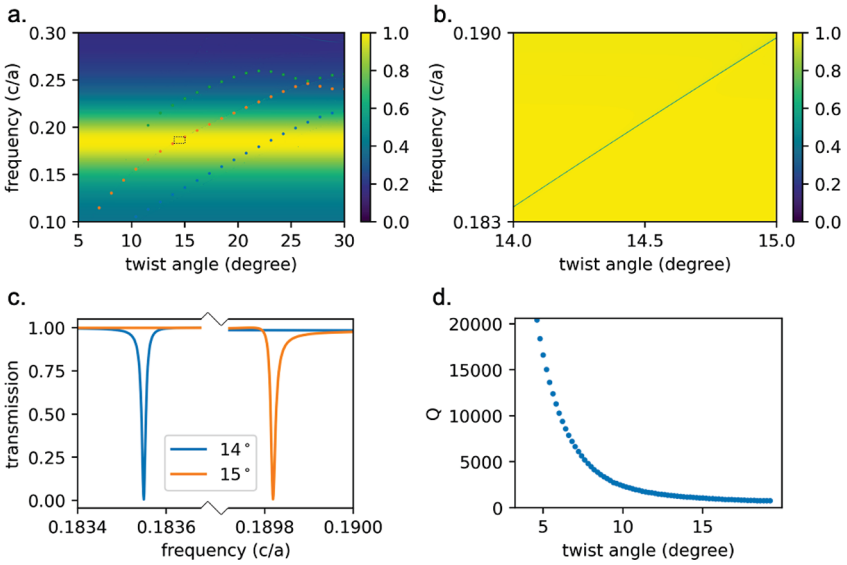

Figure 4. Properties of the structure shown in Figure 2, in the frequency range from $0.1c/a$ to $0.3c/a$. The conditions for obtaining these plots are the same as in Figure 3. (a) Transmission as a function of frequency and twist angle. The dots are the predictions of the resonant frequencies using the theory discussed in previous work.[5] (b) A zoom-in view of the region in (a) highlighted by a dashed rectangle. (c) Transmission spectra for two twist angles. (d) Quality factor as a function of twist angle, for the resonances indicated by the orange dots in (a).

To overcome the challenges as outlined above, we note that when the twist angle α is relatively small (e.g., $\alpha < 30°$), the frequencies of the lowest-order guided resonances from the Moire periodicity are significantly smaller than those from the periodicity of the individual slab, that is, $\omega_2 \ll \omega_1$, as can be seen from eqs 1 and 2. In this small-twist-angle regime, therefore, in the range of frequencies near ω_2, the only resonances come from the Moire periodicity. The frequencies of these resonances are highly dependent on the twist angle. Therefore, in this frequency range, one can achieve a clean narrow-band tunable filter response. The line shape of such tunable filters can be further engineered. For a notch filter application, for example, we want to have a near-perfect background transmission for off-resonance frequencies.[14] In the structure of Figure 2, this is achieved by introducing two extra homogeneous slabs and adjusting their dielectric constant and thickness.

In Figure 4a we plot the same quantities as in Figure 3a for the same structure shown in Figure 2, but in a lower frequency range between $0.1c/a$ and $0.3c/a$. Across the transmission spectrum there are a few curves of transmission dips resulting from the guided resonances of the system. Compared to Figure 3, there are far fewer resonances in this lower frequency range. The frequencies of all these guided resonances show strong angle dependence across a large range of twist angles. The angle dependence agrees excellently with the theory discussed in previous work.[5] All these features are consistent with the discussion above.

The transmission spectrum in Figure 4a has a frequency range near $0.185c/a$, where the transmission is largely unity, regardless of the twist angle. This effect can be accounted for by treating the photonic crystal layers as effective homogeneous slabs and by considering the Fabry−Perot interference of the resulting system.[14] The frequency range for this near-perfect transmission background could be easily tuned by varying the dielectric constant of the two homogeneous slabs in the structure of Figure 2, without affecting the frequencies of the guided resonances much (more details in the Supporting Information). Since the frequency of the guided resonance is strongly twist-angle-dependent, one can find a range of twist angles and frequencies where a set of twist-angle-dependent transmission dips pass through the near-perfect transmission background as the twist angle varies. The transmission dips along the orange dots and the blue dots correspond to lowest-order Moire resonances that originate from the guided modes of different polarizations and can both be exploited for filter application under different choices of twist angle. Within this angular and frequency range, as shown in Figure 4b, the structure operates as a tunable narrow-band notch filter, as illustrated in Figure 4c, where we plot the transmission spectrum of the structure at two twist angles. At each twist angle, the filter has near-unity background

https://doi.org/10.1021/acsphotonics.1c01263
ACS Photonics XXXX, XXX, XXX−XXX

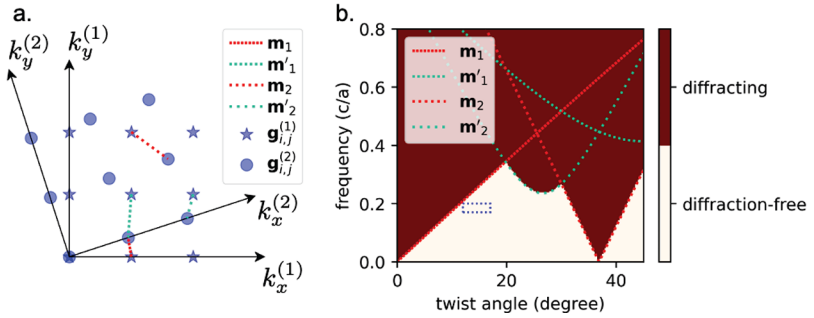

Figure 5. (a) Illustration of the leading Moire orders, where $\mathbf{g}_{i,j}^{(1)}$ and $\mathbf{g}_{i,j}^{(2)}$ denote the reciprocal lattice vectors for the two patterned layers, respectively. (b) Illustration of diffracting and diffraction-free regimes, where the dashed lines mark the boundary due to each Moire order and the dashed rectangle marks the functional parameter regime for the filter application.

transmission and near-zero transmission at the resonant dips. The resonant frequency of the filter is strongly tunable by the twist angle, and the range of tunability is far larger compared to the line width of the resonance. The ratio of tunable frequency range to line width tends to be much higher than that for conventional Fabry−Perot filters with varying incidence angles.[28] In practice, a finite beam size may lead to broadening of the filter line width (with more details in the Supporting Information).

Figure 4d shows the quality factor of the resonances, as indicated by the orange dots in Figure 4a, as a function of twist angle. We see that the quality factor also has a clear twist-angle-dependence. As the twist angle decreases, the frequency of the guided resonance becomes lower. The resonance is thus less confined in the dielectric slabs and extends further into the surrounding air region, which results in a diminishing overlap between the modal profile and the dielectric permittivity variation within the photonic crystal slabs. Since the overlap determines the leakage of the modes to the free space, the line widths of the modes become narrower as the twist angle decreases.

We note in the operating frequency range of Figure 4, our structure has almost no diffraction for normally incident light, as evidenced by the transmission reaching nearly zero at the resonance frequency in Figure 4c. For a single photonic crystal slab with a square lattice of air holes, such as that shown in Figure 1a, for normal incident light there is rigorously no diffraction for any angular frequencies below $2\pi c/a$. For the twisted bilayer structure we consider here, however, as long as the twist angle is incommensurate, the Moire wavevectors form a dense set in the reciprocal space. Therefore, in principle, at any frequency there should be diffraction, such that light incident from the normal direction can reflect or transmit in directions other than normal. However, for the low frequency range considered here, the diffraction involves a higher-order Moire scattering process and is, therefore, negligible.

To illustrate this consideration for diffraction, Figure 5a shows the set of Moire wavevectors $\mathcal{G}^{(m)} = \{\mathbf{m}_1, \mathbf{m}'_1, \mathbf{m}_2, \mathbf{m}'_2\}$ that corresponds to the lowest-order Moire scattering process. The Moire scattering process involves the scattering of light by both of the photonic crystal slabs. The process corresponding to $\mathbf{m}_1$, for example, consists of two scattering steps. Light is scattered by the first photonic crystal slab, acquiring a wavevector shift of $\mathbf{g}_{i,j}^{(1)}$ in the process, as noted in Figure 5a. The scattered light from the first slab is then scattered by the second slab, acquiring a further wavevector shift of $\mathbf{g}_{i,j}^{(2)}$, with $\mathbf{m}_1 = \mathbf{g}_{i,j}^{(1)} + \mathbf{g}_{i,j}^{(2)}$. For each $\mathbf{g} \in \mathcal{G}^{(m)}$, for normally incident light, the process is nondiffracting if $\omega < c|\mathbf{g}|$. The diffraction-free regime for the wavevectors in $\mathcal{G}^{(m)}$ is shown in Figure 5b. Our operating region in Figure 4b is thus nondiffracting for these lowest orders of Moire scattering processes. Numerically, we observe that the diffraction efficiency is less than 10^{-4} in this region when higher-order Moire scattering processes are included in the simulation. In practice, one may compromise the suppression of diffraction in favor of a larger tuning range or easier fabrication.

In this diffraction-free regime, our structure has the following polarization responses for normally incident light with a given polarization. Reflection preserves polarization. For a linearly polarized incident light, the transmission remains linearly polarized with a rotation of the polarization. As a result, circular polarizations are preserved in transmission. Both the total reflection and the total transmission, obtained by summing the outgoing power in both polarizations, are independent of the polarization of the incident light.

The polarization independence of the total transmission is numerically illustrated in Figure 6. The dielectric pattern of each photonic crystal slab in the structure of Figure 2 is C_{4v} symmetric, as shown in Figure 6a. As a result, the structure in

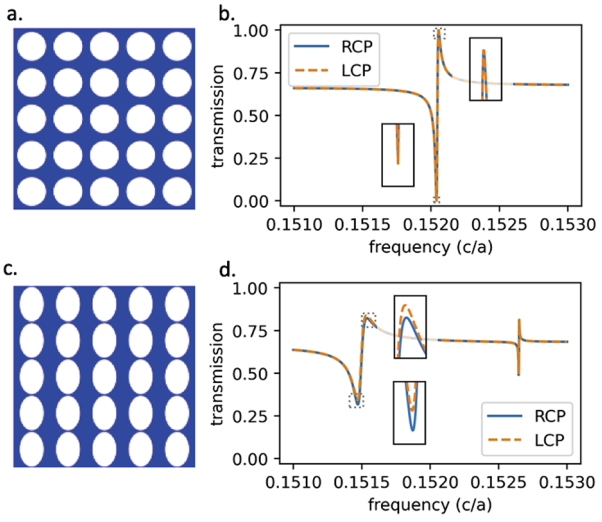

Figure 6. (a) Illustration of the dielectric pattern of the photonic crystal layers in Figure 2, which results in C_4 symmetry upon bilayer twisting. (b) Transmission spectrum at $\alpha = 10°$ for the structure in Figure 2. (c) Illustration of breaking C_4 symmetry of the dielectric pattern in (a) by stretching the hole size in y direction by a factor of 1.2. (d) Transmission spectrum at $\alpha = 10°$ for the structure of Figure 2, but using the dielectric pattern in (c) instead of (a).

https://doi.org/10.1021/acsphotonics.1c01263
ACS Photonics XXXX, XXX, XXX−XXX

Figure 2 has C_4 symmetry. The corresponding total transmission spectrum at a particular twist angle of $\alpha = 10°$ is shown in Figure 6b, where the total transmission does not differ between left-circularly polarized (LCP) and right-circularly polarized (RCP) incident light. Both full transmission and full reflection can be achieved. On the other hand, by making the dielectric pattern in each photonic crystal layer C_{2v} symmetric (Figure 6c), the corresponding total transmission spectra differ for the two incident polarizations, as shown in Figure 6d. Neither full transmission or full reflection occurs.

The polarization response discussed above can be understood from the scattering matrix description of a two-port system, constrained by C_4 symmetry, reciprocity, and energy conservation. Since the system has no diffraction, the properties of the structure, in general, can be written as

$$\begin{pmatrix} b_x^u \\ b_y^u \\ b_x^l \\ b_y^l \end{pmatrix} = S \begin{pmatrix} a_x^u \\ a_y^u \\ a_x^l \\ a_y^l \end{pmatrix}$$

Here u and l denote the upper and lower sides of the structure, x and y denote the linear polarization bases along the x and y directions, and a and b are the input and output wave amplitudes. a_x^u, for example, describes the amplitude of the x-polarized component for an input wave from the upper side of the structure.

$$S = \begin{bmatrix} R^{(uu)} & T^{(ul)} \\ T^{(lu)} & R^{(ll)} \end{bmatrix}$$

is the scattering matrix of the system. The 2×2 submatrices R and T are the reflection and transmission matrices, respectively. In the linear polarization basis, R and T can be written as

$$R = \begin{bmatrix} r_{xx} & r_{xy} \\ r_{yx} & r_{yy} \end{bmatrix}, \quad T = \begin{bmatrix} t_{xx} & t_{xy} \\ t_{yx} & t_{yy} \end{bmatrix}$$

Here all the quantities are understood to have superscripts, and we suppress the superscripts unless necessary.

Since the structure is C_4 symmetric, we have

$$r_{xy} = -r_{yx}, \quad r_{xx} = r_{yy}, \quad t_{xy} = -t_{yx}, \quad t_{xx} = t_{yy}$$

On the other hand, by reciprocity we have

$$R^t = R, \quad T^{(ul)} = [T^{(lu)}]^t$$

Therefore, we have $r_{xy} = r_{yx} = 0$. The S matrix therefore has the following form:

$$S = \begin{pmatrix} r & 0 & t & \eta \\ 0 & r & -\eta & t \\ t & -\eta & r & 0 \\ \eta & t & 0 & r \end{pmatrix}$$

Furthermore, by energy conservation, we have $SS^\dagger = 1$ and, therefore, $t^*\eta - t\eta^* = 0$. Hence, t and η have the same phase.

Based on the discussion above, we can understand the polarization properties as numerically observed. The reflection preserves polarization since the R matrix is proportional to the identity matrix, but polarization conversion does occur in the transmission process since the T matrix is not proportional to the identity. For an incident polarization $A = \begin{pmatrix} a_x^u \\ a_y^u \end{pmatrix} = \begin{pmatrix} \cos\theta \\ e^{i\phi}\sin\theta \end{pmatrix}$, the total transmission $T_{\text{total}} = \text{Tr}\{A^\dagger T^\dagger T A\}$ is independent of θ and ϕ, since t and η have the same phase. In particular, the total transmission is the same for LCP and RCP, as illustrated in Figure 6b.

$$= |t|^2 + |\eta|^2 - 4\sin\theta\cos\theta\sin\phi\,\text{Im}\{t^*\eta\}$$

CONCLUSION

We numerically demonstrate a tunable narrow-band-stop frequency filter based on twisted bilayer photonic crystal slabs. The resonant frequency of the filter is strongly tunable by varying the twist angle. The filter operates without diffraction loss and is polarization-independent. Our work points to the important opportunities of exploiting the Moire physics in twisted bilayer photonic crystal slab structures for device applications.

ASSOCIATED CONTENT

Supporting Information

The Supporting Information is available free of charge at https://pubs.acs.org/doi/10.1021/acsphotonics.1c01263.

Effect of homogeneous slabs; Effect of air gap between layers; Effect of finite beam size (PDF)

AUTHOR INFORMATION

Corresponding Authors

Beicheng Lou − *Department of Applied Physics and Ginzton Laboratory, Stanford University, Stanford, California 94305, United States;* orcid.org/0000-0001-7846-5551; Email: beichenglou@stanford.edu

Shanhui Fan − *Department of Electrical Engineering and Ginzton Laboratory, Stanford University, Stanford, California 94305, United States;* orcid.org/0000-0002-0081-9732; Email: shanhui@stanford.edu

Complete contact information is available at: https://pubs.acs.org/10.1021/acsphotonics.1c01263

Funding

This work is supported by a MURI Project from the U.S. Air Force Office of Scientific Research (Grant No. FA9550-21-1-0312).

Notes

The authors declare no competing financial interest.

ACKNOWLEDGMENTS

The authors appreciate discussions with Cheng Guo, Kai Wang, and Alex Y. Song.

REFERENCES

(1) Andrei, E. Y.; MacDonald, A. H. Graphene bilayers with a twist. *Nat. Mater.* **2020**, *19*, 1265−1275.

(2) Cao, Y.; Fatemi, V.; Fang, S.; Watanabe, K.; Taniguchi, T.; Kaxiras, E.; Jarillo-Herrero, P. Unconventional superconductivity in magic-angle graphene superlattices. *Nature* **2018**, *556*, 43−50.

(3) Hu, G.; Ou, Q.; Si, G.; Wu, Y.; Wu, J.; Dai, Z.; Krasnok, A.; Mazor, Y.; Zhang, Q.; Bao, Q.; Qiu, C.-W.; Alù, A. Topological polaritons and

photonic magic angles in twisted α-MoO3 bilayers. *Nature* **2020**, *582*, 209−213.
(4) Hu, G.; Wang, M.; Mazor, Y.; Qiu, C.-W.; Alù, A. Tailoring Light with Layered and Moiré Metasurfaces. *Trends in Chemistry* **2021**, *3*, 342−358.
(5) Lou, B.; Zhao, N.; Minkov, M.; Guo, C.; Orenstein, M.; Fan, S. Theory for Twisted Bilayer Photonic Crystal Slabs. *Phys. Rev. Lett.* **2021**, *126*, 136101.
(6) Dong, K.; Zhang, T.; Li, J.; Wang, Q.; Yang, F.; Rho, Y.; Wang, D.; Grigoropoulos, C. P.; Wu, J.; Yao, J. Flat Bands in Magic-Angle Bilayer Photonic Crystals at Small Twists. *Phys. Rev. Lett.* **2021**, *126*, 223601.
(7) Nguyen, D. X.; Letartre, X.; Drouard, E.; Viktorovitch, P.; Nguyen, H. C.; Nguyen, H. S. Magic configurations in Moiré Superlattice of Bilayer Photonic crystal: Almost-Perfect Flatbands and Unconventional Localization. *arXiv:2104.12774 [physics.optics]* **2021**, na.
(8) Guo, C.; Guo, Y.; Lou, B.; Fan, S. Wide wavelength-tunable narrow-band thermal radiation from moiré patterns. *Appl. Phys. Lett.* **2021**, *118*, 131111.
(9) Wu, Z.; Liu, Y.; Hill, E. H.; Zheng, Y. Chiral metamaterials via Moiré stacking. *Nanoscale* **2018**, *10*, 18096−18112.
(10) Wu, Z.; Zheng, Y. Moiré Chiral Metamaterials. *Advanced Optical Materials* **2017**, *5*, 1700034.
(11) Aftenieva, O.; Schnepf, M.; Mehlhorn, B.; König, T. A. F. Tunable Circular Dichroism by Photoluminescent Moiré Gratings. *Advanced Optical Materials* **2021**, *9*, 2001280.
(12) Chi, J.; Liu, H.; Wang, Z.; Huang, N. Giant optical activity in plasmonic chiral structure via double-layer graphene moiré stacking in mid-infrared region. *Opt. Express* **2020**, *28*, 4529−4540.
(13) Bernet, S.; Harm, W.; Ritsch-Marte, M. Demonstration of focus-tunable diffractive Moiré-lenses. *Opt. Express* **2013**, *21*, 6955−6966.
(14) Fan, S.; Joannopoulos, J. D. Analysis of guided resonances in photonic crystal slabs. *Phys. Rev. B* **2002**, *65*, 235112.
(15) Wang, S. S.; Magnusson, R. Theory and applications of guided-mode resonance filters. *Appl. Opt.* **1993**, *32*, 2606−2613.
(16) Kodali, A. K.; Schulmerich, M.; Ip, J.; Yen, G.; Cunningham, B. T.; Bhargava, R. Narrowband Midinfrared Reflectance Filters Using Guided Mode Resonance. *Anal. Chem.* **2010**, *82*, 5697−5706.
(17) Dang, P. T.; Le, K. Q.; Ngo, Q. M.; Nguyen, H. P. T.; Nguyen, T. K. Guided-mode Resonance Filter with Ultra-narrow Bandwidth over the Visible Frequencies for Label-free Optical Biosensor. *Journal of Advanced Engineering and Computation* **2019**, *3*, 406−414.
(18) Dobbs, D. W.; Cunningham, B. T. Optically tunable guided-mode resonance filter. *Appl. Opt.* **2006**, *45*, 7286−7293.
(19) Bark, H. S.; Jeon, T.-I. Tunable terahertz guided-mode resonance filter with a variable grating period. *Opt. Express* **2018**, *26*, 29353−29362.
(20) Macé, L.; Gauthier-Lafaye, O.; Monmayrant, A.; Calvez, S.; Camon, H.; Leplan, H. Highly-resonant two-polarization transmission guided-mode resonance filter. *AIP Advances* **2018**, *8*, 115228.
(21) Saha, N.; Kou, W.-K. Guided-mode resonance-based bandpass filter operating at full conical mounting. *Appl. Opt.* **2020**, *59*, 10700−10705.
(22) Barrow, M.; Phillips, J. Polarization-independent narrowband transmittance filters via symmetry-protected modes in high contrast gratings. *Opt. Lett.* **2020**, *45*, 4348−4351.
(23) Luo, S.; Chen, L.; Bao, Y.; Yang, N.; Zhu, Y. Non-polarizing guided-mode resonance grating filter for telecommunications. *Optik* **2013**, *124*, 5158−5160.
(24) Niraula, M.; Magnusson, R. Unpolarized resonance grating reflectors with 44% fractional bandwidth. *Opt. Lett.* **2016**, *41*, 2482−2485.
(25) Zhou, W.; Zhao, D.; Shuai, Y.-C.; Yang, H.; Chuwongin, S.; Chadha, A.; Seo, J.-H.; Wang, K. X.; Liu, V.; Ma, Z.; Fan, S. Progress in 2D photonic crystal Fano resonance photonics. *Progress in Quantum Electronics* **2014**, *38*, 1−74.
(26) El Beheiry, M.; Liu, V.; Fan, S.; Levi, O. Sensitivity enhancement in photonic crystal slab biosensors. *Opt. Express* **2010**, *18*, 22702−22714.
(27) Suh, W.; Yanik, M. F.; Solgaard, O.; Fan, S. Displacement-sensitive photonic crystal structures based on guided resonance in photonic crystal slabs. *Appl. Phys. Lett.* **2003**, *82*, 1999−2001.
(28) Lumeau, J.; Lemarchand, F.; Begou, T.; Arhilger, D.; Hagedorn, H. Angularly tunable bandpass filter: design, fabrication, and characterization. *Opt. Lett.* **2019**, *44*, 1829−1832.

https://doi.org/10.1021/acsphotonics.1c01263
ACS Photonics XXXX, XXX, XXX−XXX